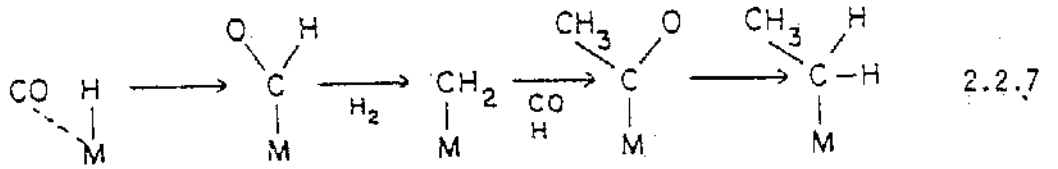

2.2.7

The intermediates involving $\overset{O}{\overset{\|}{C}}-R$ are converted to metal-alkyl species by hydrogenolysis.

Ponec (95) reviews some reaction data on some NiCu catalyst and presents some convincing support for this mechanism. NiCu alloys yield higher molecular weight products than a pure transition metal since there is more undissociated CO available on the alloys. It is well known that olefins can initiate a chain (53) but cannot readily insert as an entire C_2 species into another growing chain. CO is necessary for the growth of hydrocarbon chains since only methane is formed when CO is quickly removed from the reaction mixture (20). Exposure of a FT catalyst to sulfur resulted in a decrease in overall activity but an increase in selectivity towards the high molecular weight hydrocarbons. Based on previous surface studies (64,102) Ponec (95) suggests that the the sulfur is blocking sites necessary for CO dissociation therefore increasing the relative fraction available for CO-insertion growth.

2.3 Surface Studies on FT Catalyst

2.3.1 IR Spectroscopy

In the early 1960's Blyholder and Neff (21,22) performed " in situ" IR studies on silica supported iron using a CO/H_2 total pressure of 33 bar. They observed the growth of C-H bands during the synthesis process and claimed evidence of an C-O band. Joyner (57) later

questioned these results concluding that the data showed evidence for only C-H and O-H bands. More recently, Dalla Betta and Shelef (31) and Ekerdt and Bell (42) could not identify any C-H stretching from reaction intermediates since substitution of D_2 and H_2 did not effect the intensity of the H-derived vibrations, however, they did observe a buildup of a carbidic species during the synthesis at pressures of one atmosphere. Upon removing CO from the reaction mixture it was found that the production of CH_4 and C_2H_6 continued well after all the IR detectable CO_{ads} disappeared (41). The authors conclude that a carbon reservior is built up during the synthesis process and that the hydrogenation of this materials is a slow step in the kinetic sequence. King (63) observed a substantial amount of C-H bands in the 3000cm^{-1} region over supported Ru and Fe catalyst at pressures up to 3 bars. However, no deuterium substitution data was presented and it is uncertain whether these bands correspond to reaction intermediates (20). King (63) observed two binding sites for CO, where the weaker one was more reactive towards hydrogen.

Needless to say to date "in-situ" IR investigations have proved to be rather inconclusive. Biloen and Sachtler (M1) offer the following summary of results.

1) Oxygenated surface complexes have too low a surface concentration to be detectable. This conclusion makes sense if one agrees that the oxygenated intermediate is present at high pressures as indicated by Nijs and Jacobs (87).

2) IR experiments have predominantly been conducted at low pressure where methane is the dominant product. Perhaps the C-H bands of growing chains are not detectable under these conditions.

3) The carbidic intermediate does not give rise to C-H bands observable by IR spectroscopy due to band broadening.

2.3.2 Electron Spectroscopies

There is a host of literature concerning the application of various UHV surface spectroscopies to the study of CO hydrogenation. This brief presentation will only highlight some of the more pertinent investigations involved with identifying reaction intermediates.

Krebs et al. (66) and Bonzel and Krebs (23) performed XPS and AES studies on a clean iron (110) surface. The crystal was exposed to a CO/H_2 at 1 atm at temperature between 460-750 K and then quickly cooled in CO/H_2 flow and transferred into the UHV chamber. After exposure to the feed gas three identifiable carbonaceous layers were observed. Through line shape analysis the authors conclude that the three layers range from graphitic carbon to a polymeric CH_x species (23). The partially hydrogenated carbidic carbon could only be formed by exposure of the surface to the CO/H_2 mixture or a hydrocarbon environment. Because of the large width of the C_{1s} peak the authors conclude that there is a variety of different hydrocarbon species of the form C_iH_j where $j \geq i$. It is important to note that the authors (23) do not rule out the possibility of oxygenated carbon species on the surface. The C_{1s} spectra was skewed well into the binding energy region of carbon bonded oxygen.

Transient studies on Fe and Ru single crystals (23, 40) have shown that initially clean surfaces build up a multi-layer carbon deposit as the synthesis reaction proceeds. The methanation reaction results from

the hydrogenation of this carbon deposit. Decline in the catalytic activity results from the formation of graphitic carbon (23, 40). The amount of each type of carbon layer deposited depends upon the reaction temperature and feed ratio (23, 38, 39, 64).

Bertolini and Imelik (17) combined high resolution electron energy loss spectroscopy (HRELS), LEED, thermal desorption and work function measurements to study the H_2-CO interaction on a Ni (111) surface. The LEED pattern of the CO exposed surface at 25°C was determined to be that of a surface carbide. TPD measurements revealed that CO is more weakly held on a carburized surface as compared to a clean metallic one. These results agree with King (63) who observed a weakly bonded adsorbed CO species on a supported Ru catalyst in a CO/H_2 environment. At room temperature on the metallic surface only coadsorbed CO and H species were observed; however, upon cooling from 140°C to 25°C in CO and H_2, the carbide surface revealed the presence of oxy-carbon species. Energy loss spectra yielded the most probable forms to be

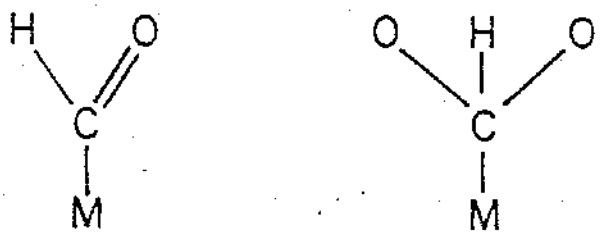

Reheating the carbide surface to 200°C yields energy loss peaks corresponding to those of a methylene species ($-CH_x-$).

2.4 Hydrogenation/Isomerization Reaction Mechanisms

Fischer Tropsch product distributions obtained at high CO conversions always contain a substantial amount of saturated straight chained paraffins in addition to α- and β-olefins. Fridel and Anderson (47) concluded that the α-olefins were the primary synthesis products since

the relative amount of primary olefins compared to secondary olefins exceeded that corresponding to thermodynamic equilibrium. Pichler et al. (94) confirmed this conclusion by showing that the α-olefin product fraction increases with decreasing CO conversion (increasing space velocity). At higher CO conversions the α-olefins were transformed via secondary reactions into β-olefins, linear paraffins and branched products (93,94).

It would seem that the hydrogenation activity of the catalyst can affect the olefin product distribution. Metal catalyzed hydrogenation is typically zero or negative order in the partial pressure of the olefin and first order in hydrogen partial pressure (48). Turkevich et al. (116) studied the hydrogenation of ethylene (Eq. 2.4.1).

$$C_2H_4 + H_2 \rightarrow C_2H_6 \qquad 2.4.1$$

They proposed the following mechanism shown below

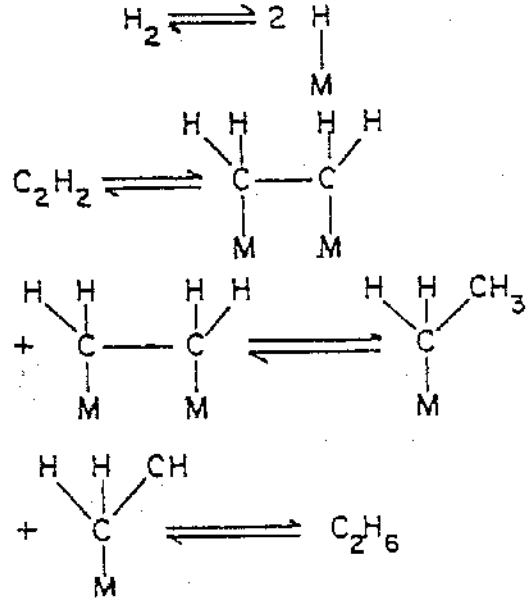

2.4.2A

2.4.2B

2.4.2C

2.4.2D

The authors (116) found a considerable amount of H-D exchange during the reaction, indicating the adsorption occurs on both carbon atoms. Infared spectra showed evidence of a "half hydrogenated" adsorbed species shown in steps 7c and 7d (41).

Ragaini (98) observed an extensive amount of double bond isomerization in conjunction with the hydrogenation of 1-butene. Gates (48) has generalized the 1-butene isomerization mechanism of Raigaini (98) as follows

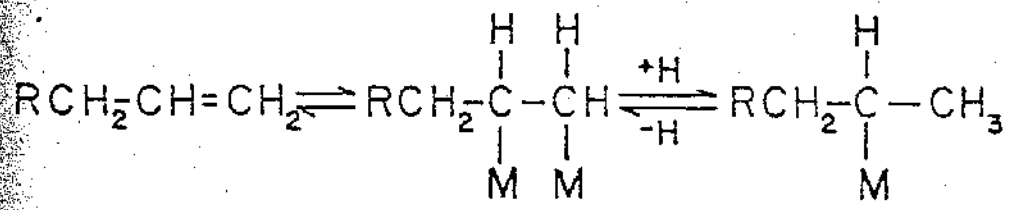

2.4.3A

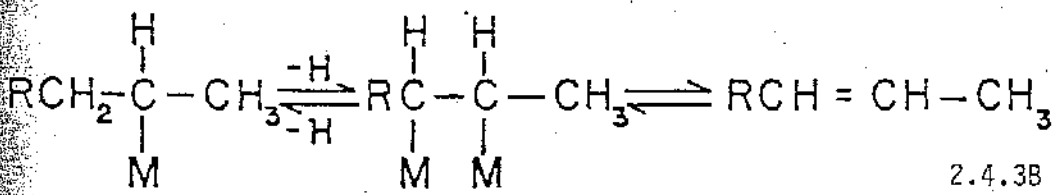

2.4.3B

It has been documented in the literature that olefins added to a CO/H_2 feed will hydrogenate, and isomerize. Pichler and Schulz (92) found that over 90% of the radioactive propylene added to a 1/2 CO/H_2 mixture hydrogenated. They employed a precipitated iron catalyst at a total pressure of twenty atmosphere. Nijs and Jacobs (87) added 1-butene to a

2/3 CO/H_2 feed and passed it over supported Co catalyst at 10 atmospheres. They observed that almost 10 times more 1-butene isomerized as compared to the amount that hydrogenated. The presence of secondary olefins and saturated hydrocarbons due to secondary reactions raises some interesting questions concerning the nature of the catalytic sites in the overall synthesis process. Are the same sites responsible for hydrocarbon chain growth as well as isomerization and hydrogenation? This question will be explored in Chapters 5 and 6.

Chapter 3

Experimental Methods and Catalyst Characterization

The three principal catalysts employed in this work consist of iron and/or cobalt supported on silica. They were originally prepared by Unmuth et al. (117, 119) and a brief discussion of the preparation technique is given in section 3.1. Extensive physical and chemical characterization studies have been performed on these catalysts by Unmuth et al. (117-119) and Amelse et al. (1,3,5) and in section 3.2 a review of their results is presented. Mossbauer Effect spectroscopy (MES) has been employed as a principal technique in the characterization studies and since it is not a well known tool of catalytic chemistry, a brief review of the theory and applicability of this technique is presented in section 3.2.1. MES studies conducted in the present investigation are presented in conjunction with the previous results (1,3,5,117-119). In section 3.3 a detailed description of the experimental apparatus and procedures employed in the reactor study is given.

3.1 Catalyst Preparation

The catalysts used in this study are supported on Davidson 62 silica gel (80/120 mesh) and were prepared by Unmuth (117-119) via nitrate impregnation to incipient wetness. Table 3.2.1 gives the nominal metal loading on a weight metal basis

Table 3.1.1 Catalysts Loadings

Catalyst	Loading (wt % metal)(1)
Fe	4.94
Co	4.61
FeCo	3.85 (Fe) 1.02 (Co)

(1) From reference 116

After impregnation the catalysts were dried for 8 hours at 125°C in air and calcined (in air) for 2 hours at 250°C and 4 hours at 450°C (119). In each case the catalysts were converted completely to oxide phases and were stored in this state for later use (3,5,119). Prior to use in the FT synthesis reaction, each catalyst was reduced in flowing hydrogen at 425°C for 24 hours. Physical and chemical characterization studies were conducted on each catalyst in both the oxide and reduced state, as well as catalyst after exposure to synthesis conditions.

3.2 Characterization Methods and Results

In this section a brief review is presented on the experimental techniques and results encountered in the characterization studies for the catalyst. The author apologizes for any inconveniences derived by the rather lengthy and detialed discussion on the theory of the Mossbauer technique. However due to the rather complicated nature of this phenomenon and its limited applicability it was throught better to risk being "overthorough" in the presentation of the technique.

3.2.1 Mossbauer Spectroscopy - Theory and Experimental

3.2.1.1 Theory

A principal and rather unique method used in the characterization of supported iron and iron alloy catalysts is the Mossbauer effect. This phenomenon involves the recoilless emission and absorption of γ-rays associated with nuclear transitions. The Mossbauer effect has been observed for 71 isotopes belonging to forty elements (49). Fortunately most of the past and present research deals with the ^{57}Fe isotope due to

the inherent properties of this element. The following discussion is provided in order to give a brief overview of the important theoretical aspects of Mossbauer Effect Spectroscopy (MES) and how they relate to the characterization of supported iron catalyst. More comprehensive treatments can be found in the references (12,32,38,49,126) which are the basis of the present text.

MES involves the recoil free emission and resonant absorption of low energy γ-rays. In order for resonance to occur there must be a finite overlap of the emitter and absorber energy levels. These energy levels are defined by the uncertainty principle in terms of the energy distribution linewidth (Γ) and half life (τ) of the excited state.

$$\Gamma_\gamma > h/2\pi \qquad 3.2.1$$

where h is Planck's constant.

The intensity distribution of the emitted γ-rays has been found to be Lorentzian and can be described by the relationship

$$I(E) = \kappa\,(\Gamma/2\pi)\,\left(\frac{1}{(E-E_0)^2 + (\Gamma/2)^2}\right) \qquad 3.2.2$$

where E_0 is the energy value corresponding to the maximum intensity and κ is a constant.

For a nucleus at rest at the instant of the transition the recoil energy E_R is given by

$$E_R = \frac{(E_0)^2}{2MC^2} \qquad 3.2.3$$

where M is the mass of the nucleus and C is the speed of light.

A classical momentum balance written in the direction of the γ-ray emission shows that the energy available to the emitted γ-ray is

$$E_R = E_0 - 2E_R \qquad 3.2.4$$

The emitted γ-ray will have its energy lowered by twice the recoil energy. The natural linewidth of low energy γ-rays is on the order of 10^{-8} ev while the recoil energy for a typical free nucleus is approximately six orders of magnitude larger. Consequently there is no possibility of resonant absorption of the photon emitted by the free nucleus, since there is no appreciable overlap of the energy distribution for the emitted and absorbed γ-ray.

When the nuclei (both absorbing and emitting) are bound in a solid, the individual recoil energy is distributed throughout the solid lattice. The energy available for the emitting the γ-ray is given by

$$h\nu = E_0 - \Sigma_i \; h\omega_i \qquad 3.2.5$$

where $\Sigma_i h\omega_i$ represents the energy of phonons that are created in the lattice via the creation of additional vibrational modes. If no energy is lost by phonon creation all of the nuclear transition energy is available to the emitted γ-ray. The zero-phonon process is aptly called recoil-free emission and is the central theme of the Mossbauer effect.

The probability of recoil-free γ-ray emission can be expressed in the same manner as the Debye-Waller factor in X-ray scattering. This Debye-Waller factor in MES can be explained in terms of the frequency modulation of γ-radiation by the vibrational motion of the nucleus around its equilibrium position. It is commonly referred to as the recoil-free fraction and is designated by the symbol f.

Using classical electromagnetic wave theory and a Debye model for the solid lattice (32), the recoil free fraction can be given by

$$f = \exp\left[-E_R/k\,\theta_0\left[\frac{3}{2} + \frac{\pi^2 T^2}{\theta_0^2}\right]\right] \qquad 3.2.6$$

where θ_0 is the Debye Temperature

k is the Boltzmam constant

T is the absolute temperature

MES is an invaluable tool in the identification and characterization of various elements for which recoil-free emission can occur. Since the effect involves the detection of shifts in nuclear trnasitions it is sensitive to both the chemical and magnetic environment of the nucleus. Perturbations in these environments manifest themselves into three experimentally measurable parameters. They are as follows

1) Isomer Shift (δ)

2) Quadrupole Splitting (ΔE_q)

3) Magnetic Hyperfine Splitting (H).

Isomer Shift:

Because an atomic nucleus occupies a finite volume, s-electrons can penetrate this nuclear volume developing an electrostatic interaction.

This interaction creates a slight shift in the nuclear energy levels as depicted in Figure 3.2.1. The nuclear energy shift, termed isomer or chemical shfit (δ) can be used to characterized the chemical state of Mossbauer nucleus. Quantum mechanics (49) can derive the origin of this shift in terms of electron wave functions and nuclear properties; however, for this work it will suffice ot make use of this shift only as method of characterization. The isomer shift of a Mossbauer nucleus can be used to identify the valence state of the element. For example for ^{57}Fe it is found that

$$\delta_{Fe}^{\circ} < \delta_{Fe}^{3+} < \delta_{FE}^{2+}$$

Since the chemical bonding of iron affects the s-electron density at the nucleus, the isomer shift can be used to identify the chemical state of the iron nucleus.

Experimentally the isomer shift is determined by measuring the displacement of a resonance peak with respect to the zero relative velocity of a reference materials, as shown in Figure 3.2. In this work the reference material is an NBS Iron foil.

Quadrupole Splitting:

In general the isomer shift is usually explained by the electrostatic interaction of a spherically symmetric nuclear charge distribution with the s-electron cloud. However, in many nuclei this nuclear distribution is asymmetric and the resultant interaction becomes more complex in nature. Nuclear energy states that lack spherical or cubic symmetry losec their degeneracy. The Quadrupole Splitting (ΔE_q) refers to the energy separation brought about lifting of the energy degeneracy. These

Figure 3.2.1

Nuclear Transitions in ^{57}Fe resulting in the observable Mössbauer Parameters

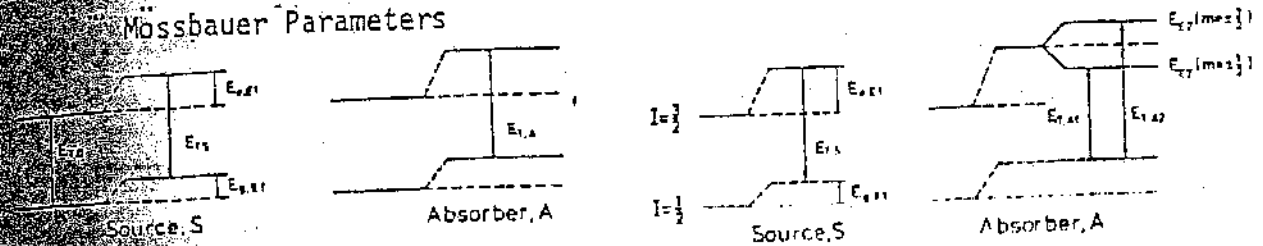

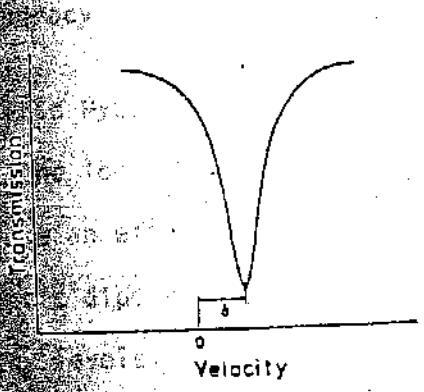

Isomer Shift (δ)

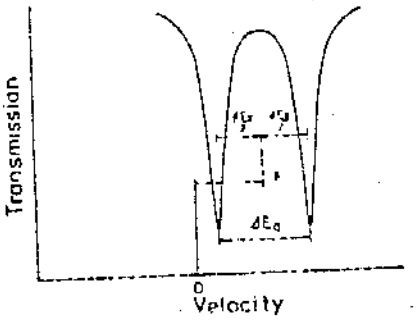

Quadrupole Splitting (ΔE_q)

Magnetic Hyperfine Splitting (H)

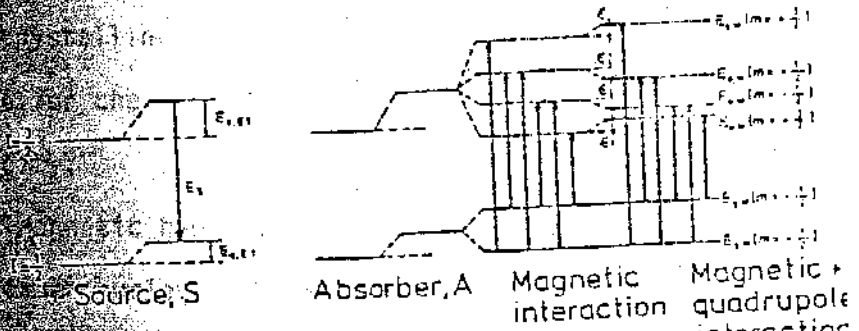

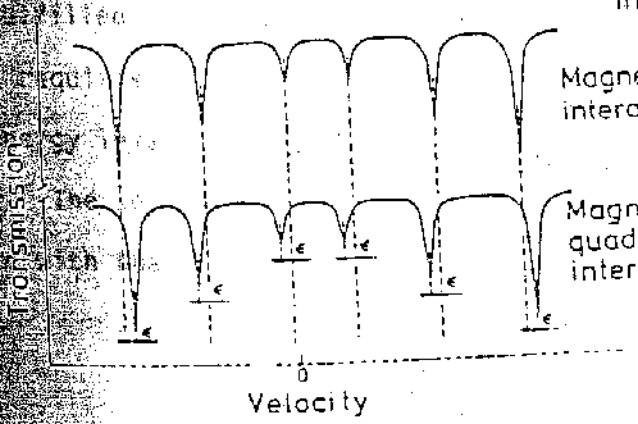

resultant energy levels for the ^{57}Fe nuclear states are shown in Figure 3.2.1 combined with the isomer shift. When the Mossbauer Nucleide is in an axially symmetric electric field (i.e., cubic) the value of ΔE_q vanishes to zero. For paramagnetic ^{57}Fe in a noncubic local environment the single absorption peak will split into two lines due to the nuclear energy level degeneracy as shown in Figure 3.2.1.

Magnetic Hyperfine Splitting:

The local chemical environment about the Mossbauer nucleus will produce an effective magnetic field that will interact with the nuclear magnetic dipole moment resulting in a further splitting of the nuclear energy levels. This interaction is termed magnetic hyperfine splitting and is shown along with the isomer shift and quadrupole splitting for ^{57}Fe in Figure 3.2.1.

For ^{57}Fe, the six resonance peaks result from the effect of internal magnetic field on the nuclear level, (Figure 3.2.1). For a polycrystalline absorber of ^{57}Fe at random orientations the intensity ratio for the six lines is 3:2:1:1:2:3 going from low velocity to high velocity.

Magnetic hyperfine interaction may sometimes not be observed for a Mossbauer nucleus possessing an internal magnetic field. Two conditions must be fulfilled in order to observe this interation (38). The first condition requires that the energy difference between the degenerate nuclear energy levels must be greater than the linewidth of the emitted gamma ray. The second condition requires that the rate of fluctuations associated with the direction of the internal magnetic field be long

compared with the observation time (τ_L) needed to observe the interaction of this field with the nucleus. This condition may be written as

$$\tau_H \geq \tau_L \qquad 3.2.7$$

where τ_H is the characteristic time associated with the magnetic relaxation (fluctuation) of the internal field. This condition and its subsequent consequences on the Mossbauer spectrum have been developed theoretically by Wickman et al. (127). The observation time (τ_L) can be regarded as the Larmor precision time, being on the order of 10^{-8} sec for ^{57}Fe (124).

In general, the direction of the internal magnetic field (M) depends upon the energy associated with that direction. There are low energy directions in which M will preferentially lie, and flipping between these directions is accomplished by crossing the magnetic anisotropy energy barrier. In the absence of an externally applied magnetic field, only thermal energy can cause the directions to flip. In ferromagnetic and antiferromagnetic materials the magnetic moments of all nuclei are coupled, hence they must collectively flip. When the magnetic domain size for these materials decreases the energy involved in flipping the coupled moments decreases and the flipping rate increases; hence small particles may not exhibit a magnetic hyperfine field in the Mossbauer spectrum. This paramagnetic behavior is termed superparamagnetism. The magnetic relaxation time becomes dependent upon domain size as the latter decreases. Consequently for a given magnetically ordered material, small particle sizes will yield a paramagnetic spectrum while larger particles will exhibit magnetic hyperfine splitting (38). By comparison of experimentally obtained Mossbauer parameters with literature values one can deduce the chemical state of the iron nucleus and infer the chemical

nature of non-Mossbauer nuclei by changes in the ^{57}Fe parameters.

If one knows the values of the recoil free fraction (f) for a particular Mossbauer nucleus in each chemical state observed in the spectrum, one can calculate the distribution of environments associated with this nucleus (12). For two different chemical environments 1 & 2, the relative ratios for a thin absorber can be expressed as a function of the spectral area associated with each environment via the relation

$$\frac{N_1}{N_2} = \frac{f_2 A_1}{f_1 A_2} \qquad 3.2.8$$

where N_1, N_2 is the number of Mossbauer atoms in environments 1 and 2.

f_1, f_2 is the recoil-free fraction for environments 1 and 2.

A_1, A_2 is the measured spectral area associated with chemical environments 1 and 2.

3.2.1.2 Mossbauer experimental

The Mossbauer data were obtained with an Austin Science Associates S-600 spectrometer. The radioactive source consisted of ^{57}Co (Amershau Co.) diffused into a rhodium matrix. Futher details on the system electronics may be found elsewhere (4,5,117,118). All spectra presented in this study were obtained in transmission geometry with the spectrometer operating in the flyback mode. Since the source was moved relative to the absorber (sample), a parabolic background appeared as the source to detector distance would change. This parabolic background was usually subtracted out during the computer analysis of the MES spectra. Details on the computational method involved in the computer analysis are given elsewhere (1,119).